2014 IEEE International Conference on
Automation Science and Engineering (CASE)
Taipei, Taiwan, August 18-22, 2014

Continuum Worm-like Robotic Mechanism with Decentral Control Architecture

Martin Eder[1], Maximilian Karl[1], Alois Knoll[1] and Stefan Riesner[2]

Abstract— **Flexible continuum robots are utilized for operational areas, in which discretely structured robots are not suitable due to their kinematic limitations. Continuum mechanisms feature adaptiveness, which is a prerequisite for constrained spaces. Furthermore, such robots can be integrated within human-robot interaction scenarios. The crucial contribution of this work is a novel intrinsic continuum worm-like robot based on a modular and decentral control architecture. It is actuated by pneumatic artificial muscles (PAMs), which result in an inherently compliant robotic system. To realize the modularity, the setup deploys a central air supply that feeds locally arranged valve cluster units, which are connected with short stub lines. Keeping the supply tubes between the valves and the PAMs short, guarantees a very direct control with good precision. This paper presents an implementation of a continuum robot with four segments comprising twelve degrees of freedom.**

I. INTRODUCTION

Conventional manipulators are based on a serial arrangement of rigid links with driven joints. They can be controlled precisely and are available for a wide range of payloads. Nevertheless, these discrete robot structures have limitations in terms of maneuverability, i.e. their kinematics have a very limited number of degrees of freedom (DOF) [1]. The rigid links and joints also cause problems when it comes to collaboration modes between humans and robots. Different kinds of methods are necessary for safety design [2], which is particularly interesting in the service robotics domain. Statistical projections for the period until 2016 estimate that about 22 Million units of service robots will be sold for personal use [3]. In this sense, the idea of safe human-robot interaction becomes more and more important.

In contrast to traditional manipulators there are continuum robotic mechanisms, which theoretically offer infinite DOF and thus high maneuverability [1], [4], [5], [6]. If these robots are actuated using flexible driving means, such as pneumatic artificial muscles (PAMs), the resulting inherent compliance meets safety requirements [7]. PAM-based robots have variable stiffness and consequently various force boundary conditions can be fulfilled.

A. Prior Art

Continuum robots [8], [9], [10] can be divided in extrinsic and intrinsic designs. Within intrinsic continuum robots the actuators are part of the support structure [4], extrinsic systems separate the drives from the backbone [11]. PAMs are efficient actuators for use in intrinsic continuum robots [9].

In the past, various embodiments of PAM-driven continuum robots have been developed. In 2004 Pritts and Rahn [12] introduced a continuum robot with two sections. The first section uses eight opposing contracting/extending PAMs, the second one six PAMs. Bartow et al. [13] built a contractor muscle based continuum trunk manipulator, also known as the *Octarm*, which comprises three sections. Each section connects three parallel PAMs. Even if the distal section utilizes smaller PAMs, the setup can be seen as a quasi-modular robot.

Additionally to PAM-based continuum robots, it is worth mentioning another interesting robot, which is based on plastic bellows manufactured with 3D printing technology. The *Bionic Handling Assistant*, developed by Festo AG & Co. KG, is one of the most lightweight continuum robots with a high power-to-weight ratio [5], [6]. It consists of three segments. The proximal segment has the largest cross section, the distal segment is designed with the smallest cross section, i.e. the overall arm is slightly cone-shaped.

B. Limitations and Solutions

Due to the high number of actuators and the different arrangement of these actuators within the two sections, the continuum robot according to Pritts and Rahn [12] is bulky and not modular. Furthermore, all muscles are switched by simple binary solenoid on/off valves, which also limits the control performance of the system. The rather bulky valves of the *Octarm* robot (proportional valves SMC ITV1050) are housed in a basement, i.e. all air supply hoses are installed inside the sections and inside the PAMs [13]. Thus, the overall number of sections is limited, as the hose feedthrough would result in great effort and larger diameters of the sections. In [14] it can already be seen that a modified version of the *Octarm* named type *IV*, which comprises four sections, doesn't contain all hoses internally, but the hoses for the distal end bypass the third section. The *Bionic Handling Assistant*, which was referenced as a crucial representation of the state of the art, also has the problem of a consistent modularity. Each segment looks different, and similar to the *Octarm*, all supply hoses are installed in a feedthrough arrangement and the large-size valves (proportional valves Festo VPWP) are located in the basement.

As a result, all systems of prior art have limitations in terms of either modularity or construction volume. In the case that an application requires a multi-segment setup, the

[1]Martin Eder, Maximilian Karl and Alois Knoll are with Faculty of Informatics, Robotics and Embedded Systems, Technische Universität München, D-85748 Garching bei München, Germany ederma@in.tum.de

[2]Stefan Riesner is with Robotics Technology Leaders GmbH, D-81247 München, Germany s.riesner@rtleaders.com

978-1-4799-5283-0/14/$31.00 ©2014 IEEE

robots mentioned above are not suitable. The major issue of current pneumatically driven intrinsic continuum robots is caused by the central placement of the valve cluster in the basement of the system. This structure leads to great effort regarding wiring and hose installation. It is impossible to build mutli-segment robots, as the plurality of supply tubes would handicap proximal segments. In addition, the overall construction size of these proximal segments would increase.

The problem as discussed before can be solved by a decentral control architecture. The idea is to equally equip each segment with both actuator and control components. All segments include the PAMs, valves, feedback sensors as well as the control hardware on board. Every segment looks exactly the same, which guarantees modularity, and it is not longer necessary to care about lots of supply tubes, since there is only one central supply hose. This central supply hose uses short stub lines that locally feed the valves and PAMs. In an analog manner, the wiring is based on a bus network, which reduces the cable installation effort.

C. Organization of this Paper

The paper is organized as follows. Section II outlines the design of the robot. II-A considers the kinematics analysis and II-B introduces the control strategy. The experimental part is covered in section III, which includes movement tests with respect to reachable positions, velocities and accelerations. Additionally, tests are carried out considering the forces and the control evaluation. The last section IV concludes the paper and gives an impression about future work.

II. Decentral Intrinsic Continuum Robot

The intrinsic continuum robot of this paper is a completely rebuilt version of a former discrete robotic arm [7], which was based on a rigid backbone structure with cardan joints. Its continuum design comprises four equal segments that are actuated by three parallel PAMs each. One segment can bend in two DOF and shorten/extend in a third DOF. Springs serve as sleeves for the PAMs in order to transfer compressive forces and to guide their motions. They also prevent the muscles from buckling. Two miniature proportional valves take care of switching one PAM – one for inlet and one for outlet. A pair of valves is united in a cluster including a pressure sensor. The entire unit is controlled by a pressure controller board, which is located directly next to it. Three small pressure controller boards are distributed around the central axis of each segment and one additional main controller board (Teensy 3.1 microcontroller) is responsible for superordinate control of these subordinated boards. A short stub tube connects the PAM with the cluster, which is again linked to a central air feed hose. In this manner, three clusters are built in one segment, all served from the same central air hose. Furthermore, each PAM is equipped with a stretch sensor, which detects the length of the muscle based on resistance principle. It is mounted on the spring using non-conductive plastic connectors. A serial arrangement of four identical segment leads to a continuum robotic mechanism with 12 DOF. All segments are fed by means of a common central air hose and controlled by a superordinate i^2C bus network. Fig. 1 depicts the assembly of those segments, shown in a bent configuration. Table I summarizes the most important specification data of the setup.

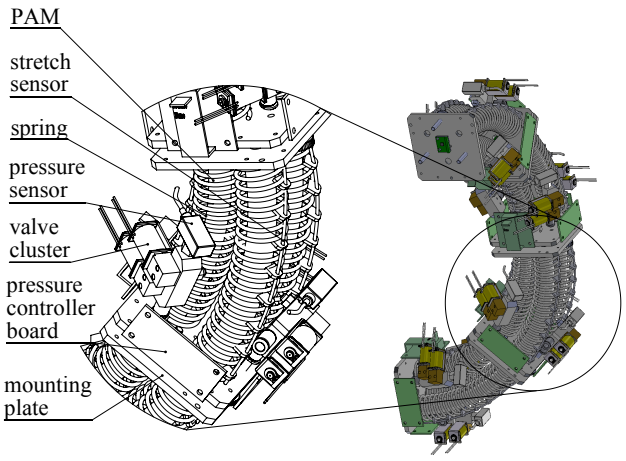

Fig. 1. Four segments of worm-like robotic mechanism

TABLE I
Mechanism specification

Feature	*Value*
Length	1008 mm
Diameter	125 mm
Segments	4
Weight	4 kg
Payload	1.2 kg
Number of PAMs	12
PAM type	Festo DMSP-10-160
Springs	30 mm × 2.7 mm, 10 mm pitch
Valves	proportional valves, Parker MD Pro
Pressure sensors	analog, SMC PSE-510-M5-Q
Stretch sensors	polymer resistor, Images SI Inc.
Segment angles	max. $\pm 30°$
Contraction	max. 120 mm
Linear velocity	max. $44\,\mathrm{m\,s^{-1}}$
Rotary velocity	max. $2100\,°\,\mathrm{s^{-1}}$
Air supply	6.9 bar

A. Kinematics Analysis

As in any type of continuum robot, the analysis of the kinematics is not a straightforward task. The main problem is dealing with the transfer of multiple DOF into a valid model with reduced computation effort. According to prior art, the estimation of the shape of a such a continuum style segment as a curved arc is a rational trade-off [4], [5], [15]. The curved arc can be modeled as a torus segment with a torus radius r_T, a torus cross section radius r_S, a torus segment angle Θ and an orientation angle Φ. Fig. 2 shows this simplification, which is in conformity with [5].

The forward kinematics can be derived by a set of three lengths l_1, l_2 and l_3, which have to be transformed to the torus approach parameters r_T, Θ and Φ. Utilizing the

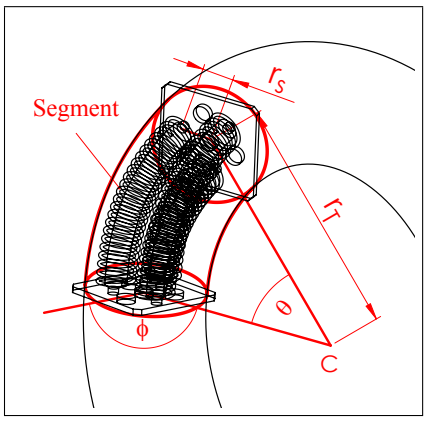

Fig. 2. Torus approach (cf. [5])

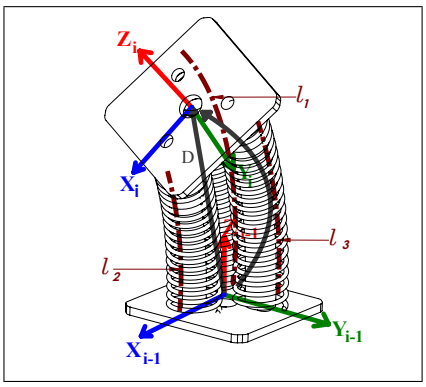

Fig. 3. Coordinate frames

correlations of [5], these parameters are identified as follows:

$$r_T = \frac{3 l_S r_S}{2g} \tag{1}$$

$$\Theta = \frac{2g}{3 r_S} \tag{2}$$

$$\Phi = \tan^{-1}\left(\frac{\sqrt{3}(l_3 - l_2)}{l_2 + l_2 - 2l_1}\right) \tag{3}$$

Equations 1 and 2 make use of a mean segment length l_S and a length squared difference term, which are calculated below:

$$l_S = \frac{\sum_{i=1}^{3} l_i}{3} \tag{4}$$

$$g = \sqrt{l_1^2 + l_2^2 + l_3^2 - l_1 l_2 - l_1 l_3 - l_2 l_3} \tag{5}$$

The overall transformation from one frame to the next frame includes both a translational part $D_{i-1}^{i}(r_T, \Theta, \Phi)$ and a rotational part R_{i-1}^{i} with

$$R_{i-1}^{i}(\Theta, \Phi) = R_z(\Phi) R_y(-\Theta) R_z(-\Phi) \tag{6}$$

The drawback of this notation is the singular case for $r_T \to \infty$, i.e. $\Theta \to 0$. This singular configuration can be treated with a replacement function $sinX$ [5] for $\alpha = \frac{\Theta}{2}$:

$$\sin X = \left\{ \begin{array}{ll} 1, & \text{if } \sin(\alpha) = 0.0 \bigwedge |\alpha| < \pi \\ \frac{\sin\alpha}{\alpha}, & \text{else} \end{array} \right\} \tag{7}$$

The corresponding term D_{i-1}^{i} yields:

$$D_{i-1}^{i}(\Theta, \Phi) = \begin{pmatrix} l_S \sin X\left(\frac{\Theta}{2}\right) \cos\left(\frac{\pi-\Theta}{2}\right) \sin\left(\Phi - \frac{\pi}{2}\right) \\ -l_S \sin X\left(\frac{\Theta}{2}\right) \cos\left(\frac{\pi-\Theta}{2}\right) \cos\left(\Phi - \frac{\pi}{2}\right) \\ l_S \sin X\left(\frac{\Theta}{2}\right) \sin\left(\frac{\pi-\Theta}{2}\right) \end{pmatrix} \tag{8}$$

This way, the corresponding coordinate transformation of one segment and consequently the arrangement of several segments can be solved, which is simply a matter of multiplication of the transformations above. Fig. 3 highlights the orientation of the frames discussed before.

Regarding the inverse kinematics, recent advances in online goal babbling approaches [16] are promising means to

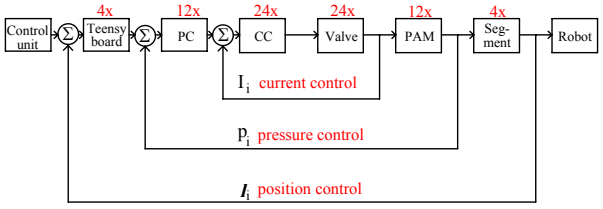

Fig. 4. Cascaded control

solve the problem of kinematically redundant multi-segment continuum mechanisms. The main idea here is to start moving all robotic segments and record the geometric effect. The algorithm starts with an inverse estimate $g(x_0, q_0)$, which is in accordance with the following equation:

$$x_t = f(q_t) \tag{9}$$

To reach a target position x_t, the necessary segment coordinates q_t are obtained with another relation:

$$q_t = g(x_t, q_t) + E_t(x_t) \tag{10}$$

that integrates a noise expression $E_t(x_t)$, which is added for performance reasons. For more on this, the reader shall be referred to [16], [17], [18], [19].

B. Control Strategy

Analog to our previous work – the discrete style robot [7] – the control strategy of the continuum worm-like robotic mechanism uses a cascaded control. In a first step, current controller stages (CC) switch the two proportional valves of each PAM. The second step integrates customized pressure controller units (PC), which set the PAM conditions considering the corresponding pressure sensor feedback. As a last step, a position loop takes the length information of all stretch sensors into account, i.e. the length information of the PAMs. Fig. 4 illustrates this cascaded control strategy.

Additionally to the singularity issue, which was already mentioned in II-A, there is another challenge regarding the length information feedback by means of the stretch sensors. The use of polymer resistor cords is extremely convenient in

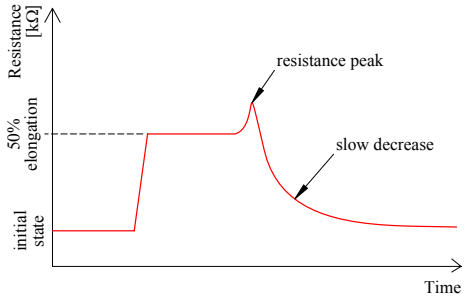

Fig. 5. Stretch sensor behavior

terms of costs, direct fixation and easy integration. Nevertheless, these sensors have a nonlinear characteristics with a hysteresis. Once they are released from a stretched configuration, the resistance has a peak before it decreases slowly, as it can be seen in Fig. 5. There is also another effect, which makes these cost-efficient sensors hard to handle: if the sensor stretches and releases several times, the overall resistance increases each time the sensor stretches. Consequently, there is effort necessary to compensate these drawbacks.

In order to control each PAM length a sliding mode controller was implemented [20], [21]. Every muscle is processed with an individual controller to follow a trajectory. In sliding mode control the system is forced to slide across a defined sliding surface. In our case this sliding surface is defined as $s(x) = x - x_d$, where x_d denotes the desired trajectory for the length of the muscle and x is the current muscle length. To ensure a sliding across the sliding manifold, $\dot{s}(x) = 0$ must be satisfied. It is assumed that the system equation for one PAM system looks as follows:

$$\dot{x} = f(p, u) \tag{11}$$

where p is the current pressure inside the muscle and u the signal representing the current in the proportional valve. For the sliding mode constraint follows:

$$\dot{s}(x) = \frac{\partial s}{\partial x}\frac{\partial x}{\partial t} = f(p, u) = 0 \tag{12}$$

This means we need to find a function $u = g(p, \dot{x})|_{\dot{x}=0}$. Values for this function were obtained by finding the maximum valve current before there is any movement, and repeating this measurement for every possible starting length of the actuator. These values were then fitted using a linear function $u_{min} = g(p)$ and used in combination with a P-controller of the form $u = u_{min} + K_p(x - x_d)$, where K_p is a parameter to adjust the weight of the error term.

III. Experiments

To demonstrate the motion capabilities of the novel mechanism, three different kinds of experiments are conducted: (A.) movement tests to identify the workspace and the limits regarding velocities and accelerations, (B.) force determination experiments and (C.) sliding mode control testing. Fig. 6 shows the experimental setup – the worm-like robotic mechanism with four segments, mounted upside down. At the flange of the robot a sensor for external motion tracking is attached, which is explained below.

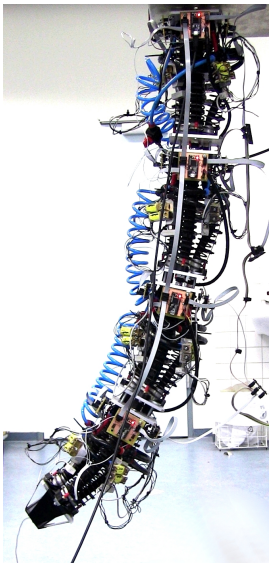

Fig. 6. Experimental setup

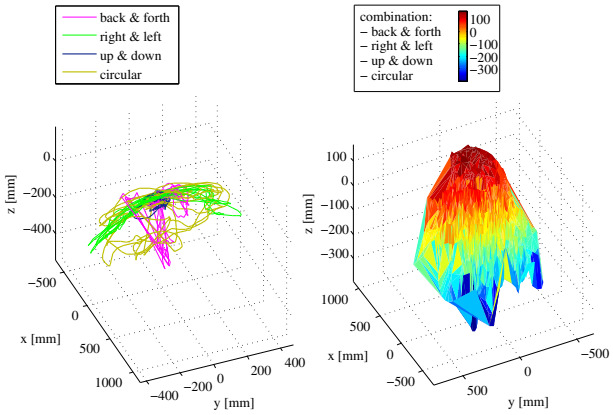

Fig. 7. Workspace

A. Movement limits

A first test series aims to identify the overall position ranges, velocities and acceleration capabilities of the flange of the continuum robotic mechanism. For these experiments an electromagnetic tracking system (3D Guidance medSAFE by Ascension Technology Corp.; 1.4 mm translational and 0.5° rotational precision) is used. A 6DOF sensor (model 180 with pre-amplifier by Ascension Technology Corp.) is attached to the distal end of the robot, which can be tracked by the transmitter of the electromagnetic tracking system. The system is deflected in arbitrary directions and moved with various minimum and maximum velocities and accelerations. Fig. 7 shows the results of the movements, which are divided in back & forth, right & left, up & down and circular motions. Examples of those movements are depicted within the subfigure on the left hand side, the combination thereof is illustrated on the right hand side, which indicates the workspace of the mechanism.

In a similar way, various randomly set positions and angles, translational and rotational position changes or velocities and accelerations were set. Corresponding recordings

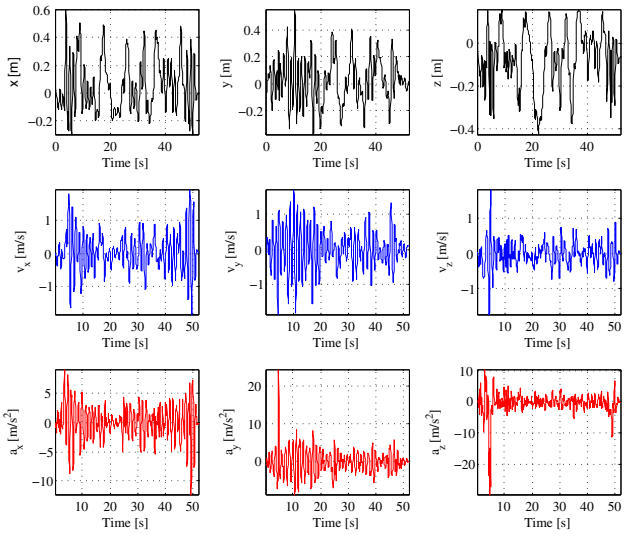

Fig. 8. Positions, translational velocities and accelerations

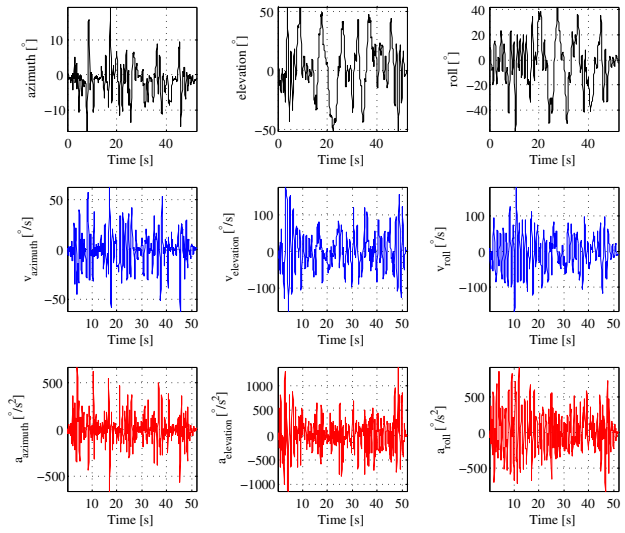

Fig. 9. Angles, rotational velocities and accelerations

for the translations are shown in Fig. 8, rotations are depicted in Fig. 9. Table II summarizes the motion capabilities of the continuum worm-like robotic mechanism. Although the PAM actuators are originally meant to generate longitudinal motions (z-direction), the setting of four segments in combination with an asynchronous control of each of the PAM triples leads to large motion ranges in x- and y-direction as well. As the mechanism doesn't have any actuation means for z-rotation, the detected azimuth angles, velocities and accelerations are only due to oscillation effects.

B. Force determination

The determination of maximum transverse forces of the mechanism are gained by means of a load cell (Phidgets CZL635), which is attached to the flange. Measured data are processed with a Wheatstone Bridge (PhidgetBridge 1046).

TABLE II
MOTION CAPABILITIES

Feature	*Value*
x	$\pm 585\,\mathrm{mm}$
y	$\pm 518\,\mathrm{mm}$
z	$\pm 342\,\mathrm{mm}$
v_x	$\pm 44\,\mathrm{m\,s^{-1}}$
v_y	$\pm 37\,\mathrm{m\,s^{-1}}$
v_z	$\pm 0.4\,\mathrm{m\,s^{-1}}$
a_x	$\pm 46\,\mathrm{m\,s^{-2}}$
a_y	$\pm 40\,\mathrm{m\,s^{-2}}$
a_z	$\pm 4.5\,\mathrm{m\,s^{-2}}$
$\phi_{azimuth}$	$\pm 19°$
$\phi_{elevation}$	$\pm 71°$
ϕ_{roll}	$\pm 65°$
$\dot{\phi}_{azimuth}$	$\pm 63\,°\,\mathrm{s^{-1}}$
$\dot{\phi}_{elevation}$	$\pm 1210\,°\,\mathrm{s^{-1}}$
$\dot{\phi}_{roll}$	$\pm 2100\,°\,\mathrm{s^{-1}}$
$\ddot{\phi}_{azimuth}$	$\pm 665\,°\,\mathrm{s^{-2}}$
$\ddot{\phi}_{elevation}$	$\pm 4770\,°\,\mathrm{s^{-2}}$
$\ddot{\phi}_{roll}$	$\pm 4010\,°\,\mathrm{s^{-2}}$

Maximum forces in longitudinal direction are based on PAM characteristics, as already shown in [7], [22]. According to these characteristics, the PAM forces strongly depend on the contraction state. Z-forces are given for two kinds of states – beginning of contraction with 0 % shortening and almost completely contracted state with 20 % shortening[1]. Results of the measurements and characteristics calculations are summarized in Table III. As the PAM actuators utilized here are designed for contraction only, it is comprehensible that the forces in z-direction – longitudinal direction – are far higher than the ones in x- and y-direction. Motions in both x- and y-directions are due to the arrangement of three PAMs and their interaction while controlled in an asynchronous mode, which results in bending.

TABLE III
MAXIMUM FORCES

Force	*Max. value*
F_{-x}/F_{+x}	7.0 N/4.7 N
F_{-y}/F_{+y}	4.5 N/4.8 N
$F_{z,0\%}/F_{z,20\%}$	1710 N/35 N

C. Sliding mode control test

Utilizing the same experimental setup as described before, tests concerning the sliding mode control approach (cf. subsection II-B) are carried out. The distal segment is moved in a sinusoidal way, which means permanent up and down motions. All length values l_1, l_2 and l_3 of the stretch sensors are recorded and compared to the sine trajectory. All length values are dimensionless with respect to the resistance output signals, which are processed with the ADC of the pressure controller boards (cf. section II). Results are illustrated in Fig. 10. On the left hand side, the waveforms are depicted, on the right hand side the relative errors between the sine function and the stretch sensor values are plotted. It can be

[1] the PAMs used can shorten up to 25 %

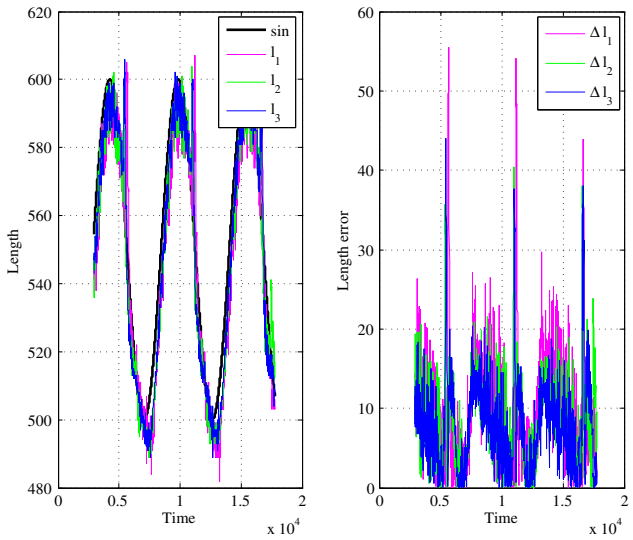

Fig. 10. Sliding mode closed loop

seen that the maximum distortion is after the turning points of the wave. In particular, there are peaks after the upper reversal point, which corresponds with the sensor behavior that was described in Fig. 5. The mean error of each length is in the range of 8.6, the standard deviation is 6.3, which is slightly better than the deviation reported in [23].

IV. Conclusion and Future Work

In this paper the concept of an intrinsic continuum worm-like robotic mechanism was introduced, which is completely modular. The control architecture is characterized by a decentral distribution of hardware components. In contrast to the control architecture, the medium supply and all wiring is centralized consistently, i.e. there is only one air hose feeding locally arranged valve clusters via stub lines and there is one cable linking all segments including i^2C bus and power supply. Within the experimental section of this paper it could be proved that the mechanism has a remarkable workspace and is able to move and accelerate fast. Furthermore, the sliding mode control approach could be introduced as a reasonable method to deal with noisy sensor signals.

In the future, the mechanism shall be expanded to a system with an even higher number of segments and DOF. The implementation of an adequate input device to control the setup is another issue that has to be addressed. Regarding the integration of components, the authors even think about replacing the current metal plates and connectors by 3D printed rapid prototyping parts (cf. [6]).

References

[1] M. W. Hannan and I. D. Walker, "Kinematics and the Implementation of an Elephant's Trunk Manipulator and Other Continuum Style Robots," In: Journal of Robotic Systems, Vol. 20, pp. 45–63, 2013

[2] J. T. C. Tan et al., "Safety design and development of human-robot collaboration in cellular manufacturing," In: Proceedings of the IEEE International Conference on Automation Science and Engineering, pp. 537–542, 2009

[3] IFR Statistical Department, VDMA, "World Robotics 2013 Service Robots Statistics, Market Analysis, Forecasts, Case Studies," 2013

[4] B.A. Jones and I. D. Walker, "Kinematics for multisection continuum robots," In: Transactions on Robotics, Vol. 22, No. 1, pp. 43–55, 2006

[5] M. Rolf and J. J. Steil, Constant curvature continuum kinematics as fast approximate model for the Bionic Handling Assistant. In: Proceedings of the International Conference on Intelligent Robots and Systems, pp. 3440-3446, 2012

[6] A. Grzesiak, R. Becker and A. Verl, "The Bionic Handling Assistant: a success story of additive manufacturing," In: Journal of Assembly Automation, Vol. 31, issue. 4, pp. 329–333, 2011

[7] M. Eder et al., "Design of an inherently safe worm-like robot," In: Proceedings of the International Symposium on Safety, Security, and Rescue Robotics, pp. 1–6, 2013

[8] G. Robinson, J.B.C. Davies, "Continuum robots - A State of the Art," In: Proceedings of the International Conference on Robotics and Automation, pp. 28492854, 1999

[9] B. Siciliano and O. Khatib, "Springer Handbook of Robotics", Springer, ISBN 9783540239574, 2008

[10] R. J. Webster III and B. A. Jones, "Design and kinematic modeling of constant curvature continuum robots: a review," In: International Journal of Robotics Research, Vol. 29, No. 13, pp. 1661-1683, 2010

[11] R. O. Buckingham and A. C. Graham, "Dexterous manipulators for nuclear inspection and maintenance – Case study," In: Proceedings of the 1st International Conference on Applied Robotics for the Power Industry, pp. 1–6, 2010

[12] M.B. Pritts and C.D. Rahn, "Design of an artificial muscle continuum robot," In: Proceedings of the International Conference on Robotics and Automation, Vol.5, pp.4742–4746, 2004

[13] A. Bartow, A. Kapadia and I. D. Walker, "A contractor muscle based continuum trunk robot," In: International Journal of Systems Applications, Engineering & Development, Vol. 8, pp. 198–206, 2014

[14] W. McMahan et al., "Field trials and testing of the Octarm continuum manipulator," In: Proceedings of the International Conference on Robotics and Automation, pp. 2336–2341, 2006

[15] B. Jones and I. D. Walker, "Limiting-case analysis of continuum trunk kinematics," In: Proceedings of the International Conference on Intelligent Robotics and Automation, pp. 1363–1368, 2007

[16] M. Rolf, J.J. Steil and M. Gienger, "Online Goal Babbling for rapid bootstrapping of inverse models in high dimensions," In: Proceedings of the IEEE International Conference on Development and Learning (ICDL), Vol.2, pp.1–8, 2011

[17] M. Rolf and J. J. Steil, "Efficient Exploratory Learning of Inverse Kinematics on a Bionic Elephant Trunk," In: Transactions on Neural Networks and Learning Systems, No. 99, pp. 1–14, 2013

[18] R. F. Reinhart and M. Rolf, "Learning versatile sensorimotor coordination with goal babbling and neural associative dynamics," In: Proceedings of the Third Joint International Conference on Development and Learning and Epigenetic Robotics, pp. 1–7, 2013

[19] M. Rolf, J. J. Steil and M. Gienger, "Goal Babbling Permits Direct Learning of Inverse Kinematics," In: Transactions on Autonomous Mental Development, Vol. 2, No. 3, pp. 216–229, 2010

[20] K. D. Young, V. I. Utkin and U. Ozguner, "A control engineer's guide to sliding mode control," In: IEEE Transactions on Control Systems Technology, Vol.7, No.3, pp.328–342, 1999

[21] A. Sabanovic, L. Fridman and S. Spurgeon, "Variable structure systems from principles to implementation," Institution of Engineering and Technology, IEC Control Engineering Series 66, ISBN 9780863413506, 2004

[22] M. Eder et al., "Compliant worm-like robotic mechanism with decentrally controlled pneumatic artificial muscles," In: Proceedings of the First International Conference on Innovative Engineering Systems, pp. 243–248, 2012

[23] V. Vibhute and A. Kshirsagar, "Identification of hysteresis and relaxation parameters in stretch sensor," In: International Journal of Advanced Electrical and Electronics Engineering, Vol. 1, pp. 15–22, 2012